Accepted Manuscript

An electrochemical paper based nano-genosensor modified with reduced graphene oxide-gold nanostructure for determination of glycated hemoglobin in blood

Seyedeh Yasaman Shajaripour Jaberi, Ali Ghaffarinejad, Eskandar Omidinia

PII: S0003-2670(19)30740-8

DOI: https://doi.org/10.1016/j.aca.2019.06.018

Reference: ACA 236860

To appear in: *Analytica Chimica Acta*

Received Date: 22 April 2019

Revised Date: 4 June 2019

Accepted Date: 10 June 2019

Please cite this article as: S.Y. Shajaripour Jaberi, A. Ghaffarinejad, E. Omidinia, An electrochemical paper based nano-genosensor modified with reduced graphene oxide-gold nanostructure for determination of glycated hemoglobin in blood, *Analytica Chimica Acta*, https://doi.org/10.1016/j.aca.2019.06.018.

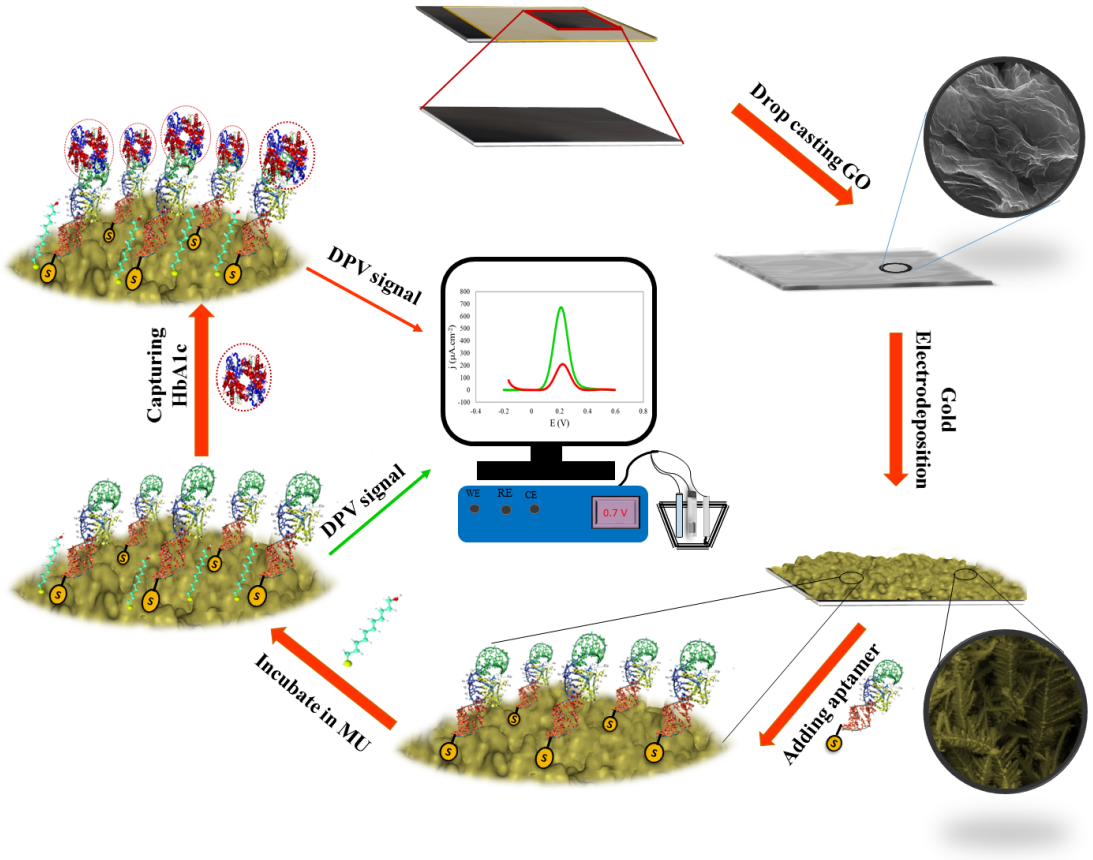

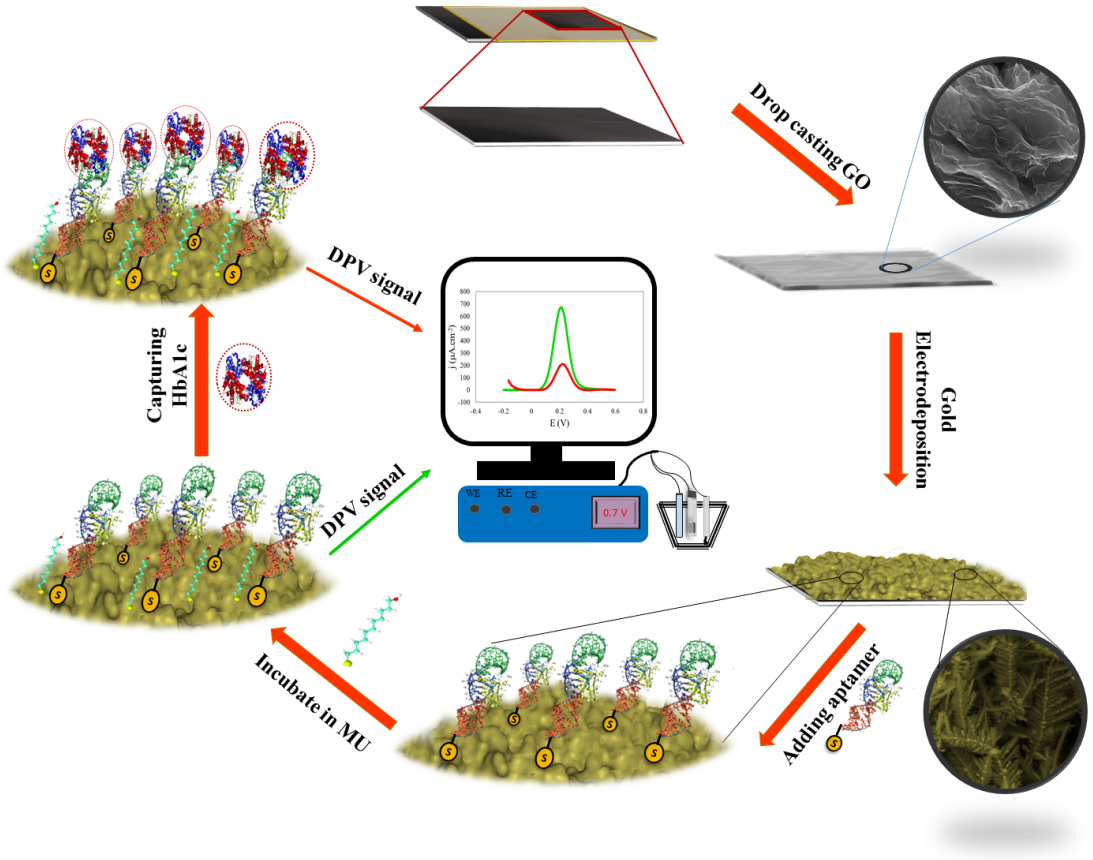

An electrochemical paper based nano-genosensor modified with reduced graphene oxide- gold nanostructure for determination of glycated hemoglobin in blood

Seyedeh Yasaman Shajaripour Jaberi[a,b], Ali Ghaffarinejad[a,b,*], Eskandar Omidinia[c,*]

[a] Research Laboratory of Real Samples Analysis, Faculty of Chemistry, Iran University of Science and Technology (IUST), Tehran 1684613114, Iran

[b] Electroanalytical Chemistry Research Center, Iran University of Science and Technology (IUST), Tehran 1684613114, Iran

[c] Department of Biochemistry, Genetic and Metabolism Research Group, Pasteur Institute of Iran, Tehran, Iran

Abstract

Hemoglobin A1c (HbA1c) is a standard biomarker to measure long-term average glucose concentration for diagnosis and monitoring of diabetes. Various methods have been reported for measuring HbA1c, however, portable and precise determination is still challenging. Herein, a new highly sensitive electrochemical nanobiosensor is developed for the specific determination of HbA1c. A nanocomposite of reduced graphene oxide (rGO) and gold with hierarchical architecture structure was electrochemically deposited on a cheap and flexible graphite sheet (GS) electrode. The nanocomposite increased the surface area, improved the electron transfer on the electrode surface and augmented the signal. It also provided a suitable substrate for linkage of thiolated DNA aptamer as a

[*] Corresponding authors:
Ali Ghaffarinejad:
Email: Ghaffarinejad@iust.ac.ir; Tel: +98-21-77240652; Fax: +98-21-73021554
Eskandar Omidinia:
Email: skandar@pasteur.ac.ir and eomid8@gmail.com; Tel: +98-21-66969298

bioreceptor on the electrode surface by strong covalent bonding. The quantitative label free detection was carried out by differential pulse voltammetry (DPV) in a phosphate-buffered saline (PBS) solution containing redox probe $Fe(CN)_6^{3-/4-}$. The detection is based on insulating the surface in presence of HbA1c and decreasing the current, which is directly related to the HbA1c concentration. The nanobiosensor demonstrated high sensitivity of 269.2 µA. cm^{-2}, wide linear range of 1 nM to 13.83 µM with a low detection limit of 1 nM. The biosensor was successfully used for measuring HbA1c in blood real sample. Furthermore, it is promising to use it as a part of a point of care device for low-invasive screening and management of diabetes.

Keywords: Electrochemical biosensing; Paper-based biosensor; Nano-genosensor; glycated hemoglobin

1. Introduction

Diabetes is a chronic disease that its prevalence is increasing rapidly with worrying pace [1]. The long-term effects of failure to control diabetes cause many complications such as cardiovascular disease and nerve, kidney, eye, foot, etc. damages [2, 3]. Therefore, early diagnosis and continuous control of the disease are urgent to the survival and the life quality improvement of millions of people throughout the world. In the recent few decades, the measurement of HbA1c, the most important glycated protein, has been identified as a standard diagnostic tool for detection, evaluation and management of diabetes. The level of HbA1c is forcefully dependent on glucose levels over the past two or three months. Consequently, the HbA1c assay is an appropriate complementary or even alternative to glucose for long term diabetes management [4]. Various laboratory

methods have been reported for HbA1c determination [5-8] among which boronate-affinity high performance liquid chromatography (HPLC), immunoassays and electrophoresis are commonly used [9-11]. However, the benefits of HbA1c determination by these methods are often offset by their high costs, time consuming, complexity of their operations and not very validity for quantitative measurements [12, 13]. Thereby, there is a demand for development of an accessible, sensitive, simple and inexpensive diagnostic method.

The use of electrochemical biosensors due to their inimitable virtues is increasing. They are the infrastructure of portable devices which provide quick results and sample analysis directly without the need to transfer it to the medical laboratory [13]. Various sensors and biosensors have been reported for measurement of HbA1c [14-18]. However, they either have a complicated preparation process or are not sufficiently sensitive. For direct measurements of HbA1c, because the heme group, the redox center of the protein, is located in the protein shell, the electron transfer is very slow making its behavior similar to a non-electroactive molecule [18]. Therefore, the signal amplification is required. For this purpose and other reasons listed below, the development of biosensors is of particular importance through the improvement of the interface between the bioreceptor and the electrode: (i) impossibility of direct linkage of the bioreceptor to the electrode, (ii) the slow kinetics of electron transfer and (iii) low sensitivity of biomolecules detection on the bare electrodes.

Because of the high surface area, high free surface energy and catalytic effects, nanostructures play an important role for the fabrication of the sensors [19-21]. Among

the nanomaterials, the integration of graphene with gold nanostructures brings excellent properties to the biosensors due to the features of each component [22-24]. Graphene oxide, thanks to its functional groups and high surface area, makes a suitable substrate available for further modification [25-27]. Strong interactions of gold nanostructures with the thiol functional group provide a potent possibility for tethering the thiolate biomolecule. They also improve electron transfer due to their excellent catalytic properties [28-32].

In this study, by adopting the electrodeposition as a straightforward procedure and controlling of the electrodeposition conditions, a three-dimensional nanostructure of gold was obtained. This nanostructure can supply more sites for the linkage of thiolated aptamer biomolecules and consequently, more biomolecules can be loaded making the nanobiosensor more sensitive. A graphite sheet (GS) was used as an electrode substrate that possesses outstanding electrical conductivity. Because of its low fabrication cost, availability and simple modification, it can be a good candidate to commercialize the biosensor. Furthermore, it can be used as a disposable electrode that does not have a pollution problem or memory effects. Ultimately, the fabricated biosensor was directly applied for the determination of HbA1c in blood samples.

2. Experimental

2.1. Chemical and reagents

DNA aptamer with a sequence of 5′-SH-TGGCAGGAAGACAAACACATCGTCGCGGCCTTAGGAGGGGCGGACGGGGGG

GGGCGTTGGTCTGTGGTGCTGT-3′ [33] was purchased from Bioneer Co (Korea). A stock solution of aptamer was prepared by dissolving it in DNase/RNase-free distilled water then maintained at -20 °C until use. The HbA1c calibrator of 3.48 and 13.83 µmol L^{-1} in the presence of Hb 100.3 and 141.3 µmol L^{-1}, respectively as standard (stock) for preparation of target solution were purchased from Pishtaz Teb Zaman Diagnostics (Iran). The other concentrations were prepared by diluting the calibrators.

Graphite powder, sulfuric acid (H_2SO_4, 98%), potassium peroxodisulfate ($K_2S_2O_8$), phosphorus pentoxide (P_2O_5), hydrogen peroxide H_2O_2, and potassium permanganate ($KMnO_4$) as reagents for GO preparation were purchased from Merck. Gold bar with purity of 99.99% was used as Au source for gold electrodeposition. 11-mercapto-1-undecanol (MU) as blocking molecule (purity 97%) was purchased from Sigma-Aldrich.

Nitric acid (HNO_3, 65%), ammonia (NH_3, 25%), hydrochloric acid (HCl, 37%), potassium nitrate (KNO_3) and cysteine were used in electrodeposition process. Phosphate-buffer saline (PBS) solution 0.01 mol L^{-1} (pH 7.4) containing an equivalent molar concentration (5 mmol L^{-1}) of potassium ferricyanide ($K_3Fe(CN)_6$) and potassium ferrocyanide ($K_4Fe(CN)_6$) probe salts were used as biosensing electrolyte. PBS solution consists of 137 mmol L^{-1} NaCl, 2.7 mmol L^{-1} KCl, 2 mmol L^{-1} KH_2PO_4 and 10 mmol L^{-1} Na_2HPO_4 was prepared in deionized water. Ascorbic acid, dopamine hydrochloride (98%), uric acid and glucose were used for assessing the selectivity. All of the above mentioned reagents were purchased from Merck.

2.2. Apparatus and Methods

Amperometric measurements were carried out with an Autolab Potentiostat/Galvanostat (PGSTAT 30). Electrochemical impedance spectroscopy (EIS) experiments were performed with a Potentiostat/Galvanostat equipped with FRA module (Autolab PGSTAT204). The amperometric and EIS data were analyzed with Nova 1.11 and ZSimpWin (version 3.40) software, respectively. The electrochemical cell consisted of a three-electrode system including Ag/AgCl (3 mol L^{-1}) reference electrode, Pt rod counter electrode and modified or unmodified GS as working electrode. The GS with thickness of 0.15 mm was purchased from Latech Scientific Supply Pte Ltd (Singapore). Characterization of electrode surface was accomplished with the following techniques and instruments: scanning electron microscopy (SEM; TESCAN/VEGA2, Czech Republic), field emission scanning electron microscopy (FESEM) equipped with energy dispersive X-ray spectroscopy (EDS) (TESCAN MIRA3), X-ray diffraction (XRD; Bourevestnik, DRON-8) and Fourier transform infrared spectroscopy (FT-IR; SHIMADZU FTIR-8400S).

2.3. Fabrication of the rGO-gold nanocomposite as substrate

A schematic illustrating the steps involved in the synthesis of rGO-Au nanocomposite on the GS, fabrication of nanobiosensor and ultimately its use for the detection of HbA1c is presented in Scheme 1. GS with the surface of 0.25 cm^2 was prepared and rinsed successively with acetone, ethanol and deionized (DI) water. GO was synthesized by a modified Hummer's method reported previously [34].

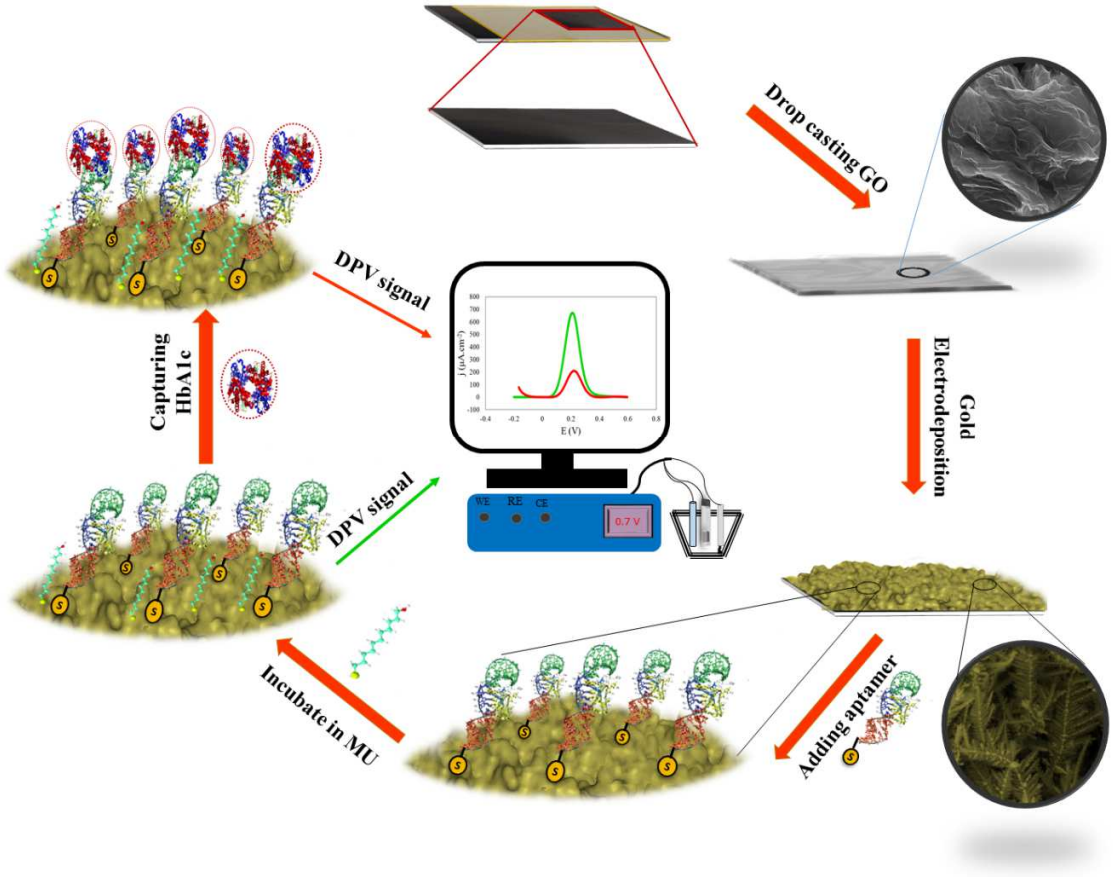

Scheme 1. A schematic representation of the main steps for modification of GS to fabricate HbA1c nanobiosensor. First, GO was cast coated on the GS and then, gold nanostructure was electrodeposited over GS/GO. Next, thiolated DNA aptamer as bioreceptor was added to the modified electrode. The electrode was then incubated in 11-mercapto-1-undecanol (MU) solution to prevent non- specific binding.In the next step, HbA1c was added to be captured with the aptamer. Finally, the capturing of HbA1c was sensed using DPV technique.

The GO with a concentration of 0.5 mg mL^{-1} was completely dispersed in DI water with the assistance of ultrasonic vibrations. Then it was dropwisely cast on the electrode surface and was allowed to dry. Subsequently, gold nanostructures were deposited over the obtained surface inspired from the previous report [35] but with a fundamental

variation in the source of gold, the electrolyte composition and the deposition process. For the preparation of a stock solution of $HAuCl_4$, 1 g gold bar was dissolved in an appropriate volume of aqua regia (a mixture of HNO_3 and HCl in a volume ratio of 1:3). A proper volume of this solution for preparing 3 mmol L of Au^{3+} was added to the electrolyte solution for electrodeposition containing cysteine (0.1 mmol L^{-1}), NH_3 (0.5 mol L^{-1}) and KNO_3 (0.1 mol L^{-1}). Prior to starting the electrodeposition process, the electrolyte solution was deoxygenated by bubbling N_2 gas for 10 min and during the process, the solution atmosphere was kept saturated with N_2. The deposition was performed by cyclic voltammetry (CV) and by applying 10 successive cycles in the potential range of -1.5 to 1 V and with the scan rate of 0.025 V s^{-1}. Then, the electrodes were dried in the ambient condition. Also, for comparison, the gold nanostructure and rGO were separately electrodeposited on the electrode surface under similar conditions in the absence of GO and Au, respectively.

2.4. Biosensor preparation and detection of HbA1c

For biosensor preparation, 40 µL of the aptamer solution with a specific concentration (1 µmol L^{-1}) was dropped on the electrode surface and left at room temperature overnight in a dark place to immobilize the thiolated aptamer onto the GS/rGO-Au electrode via covalent bonding. After rinsing the electrode with PBS, it was immersed in a MU solution (1 mmol L^{-1}) for 1 h in order to prevent non-specific binding. For HbA1c biosensing, different successive concentrations of it were prepared and 40 µL of these solutions were dropped on the biosensor surface and incubated at room temperature for 1 h. At the end, related DP voltammograms were recorded in the probe solution (a solution

of PBS (0.01 mol L^{-1}) containing 5 mmol L^{-1} mixture of $Fe(CN)_6^{3-}$/ $Fe(CN)_6^{4-}$ as redox probe). These results were compared with the control nanobiosensor (without target, i.e. GS/rGO-Au-aptamer-MU).

3. Results and Discussion

3.1. Preparation and characterization of GS/rGO-Au nanocomposite

Figure 1a and b shows the CV curves of GS/GO electrode in the regia solution containing ammonia and cysteine in the absence and presence of gold ions, respectively. By comparing these two curves, a reduction peak around 0.6 V is observed (inset of Figure 1) which can be clearly attributed to the growth of gold on the surface.

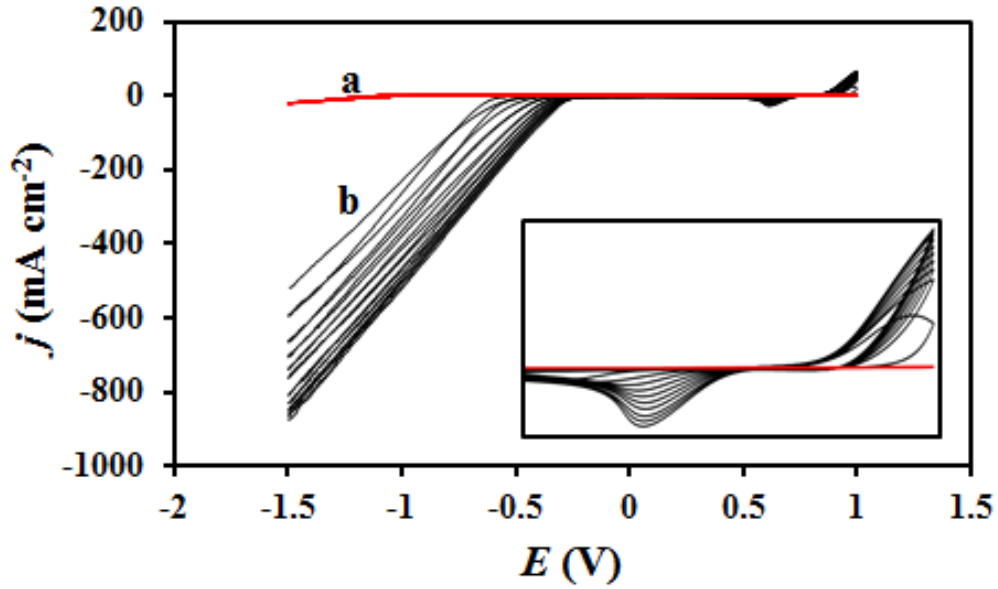

Figure 1. CV curves of electrodeposition process for GS/GO electrode in an aqua regia solution containing 0.5 mol L^{-1} NH_3 and 0.1 mmol L^{-1} cysteine in (a) the absence of gold and (b) the presence of gold. 10 cycles were applied in a potential range of -1.5 to 1 V under scan rate of 0.025 V s^{-1}. Inset: Zoom in part of plots a and b.

The increased current observed between -1 and -1.5 V can be related to the reduction of oxygen functional groups in GO [36] and also reduction of hydronium ions in the acidic solution. The higher reduction current in the presence of gold may be due to its catalytic properties to hydrogen evolution reaction (HER). Increasing the reduction current with successive cycles causes the continuous deposition of the gold and augmentation of the catalyst amount for HER. The hydrogen evolution current is so high that covers the current arising from the reduction of GO.

To investigate the structure and morphology of the electrode surface in different stages of nanocomposite preparation, the FE-SEM analysis was performed. Comparing the FE-SEM image of GS/GO (Figure 2B) with that of the unmodified electrode (Figure 2A) indicates that transparent graphene layers are clearly wrinkled on the surface. This graphene-wrinkled structure with a high surface roughness acts as a scaffold to anchor metal nanostructure preparing the surface for further modification. It also causes mechanical integrity, tensile strength and minimization of the surface energy [37]. Figure 2C and D shows the images of the final modified electrode surface (GS/rGO-Au) with two magnifications which indicates the formation of hierarchical nanostructure with hyperbranched gold dendrite. This dendritic structure is well covered the entire surface and provides a large surface area for bonding the bioreceptor molecules and also facilitates electron transfer and therefore, enhances the signal due to its excellent conductivity.

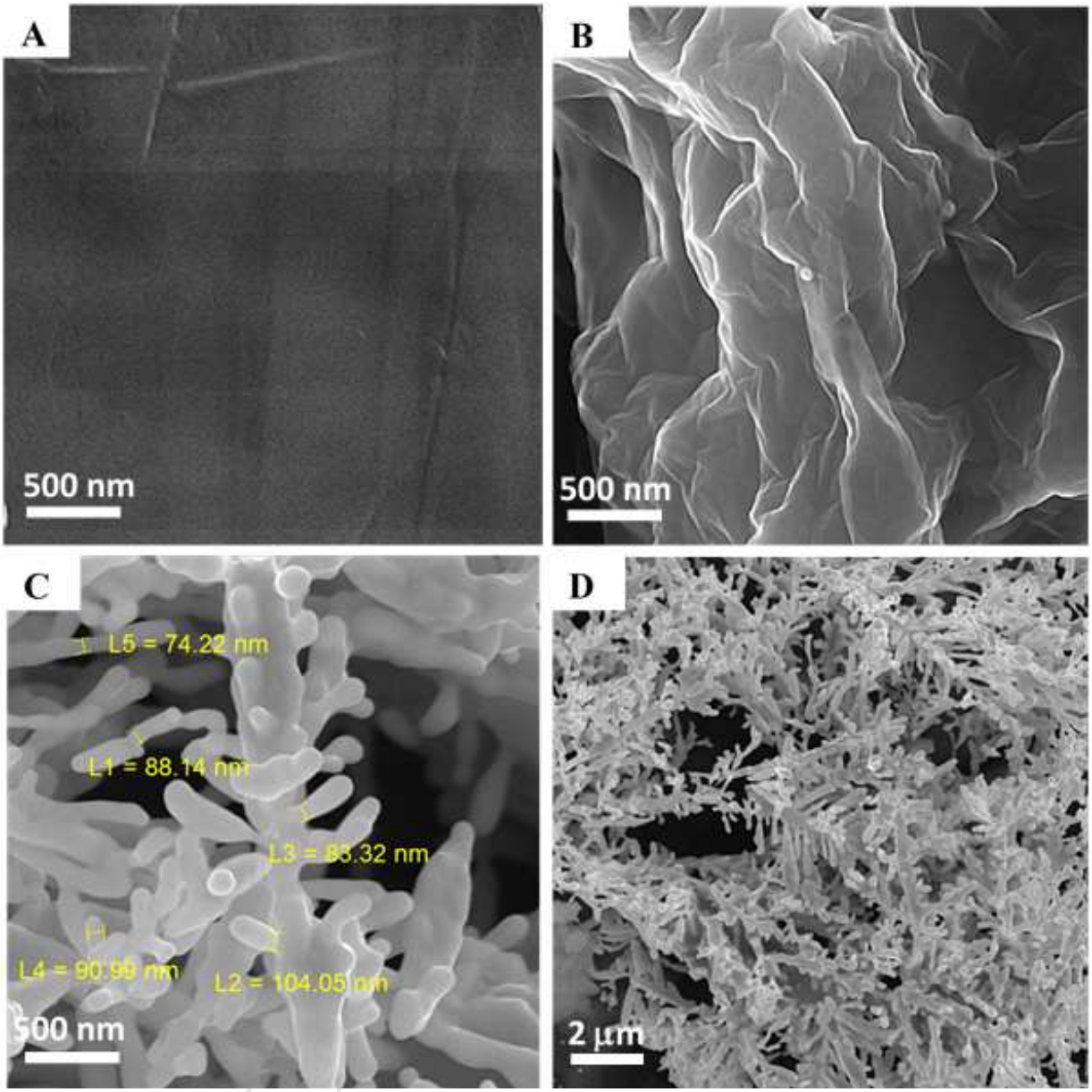

Figure 2. FE-SEM images of (A) bare GS, (B) GS/GO, (C) and (D) GS/rGO- Au with two magnifications

For further confirmation of the gold nanostructures formation, the results of the XRD and EDS tests are presented in Figures S1 and S2). The XRD pattern of the GS/GO-Au electrode surface (Figure S1b) in comparison with that of the GS/GO (Figure S1a) shows four main diffraction peaks at 2θ angels of 39.4, 45.6, 65.8, and 78.8° which are

attributed to the (111), (200), (220) and (311) planes of cubic Au, respectively. This diffraction data are in good agreement with the 00-001-1172 JCPDS card. Furthermore, the EDS analysis (Figure S2A) confirms the presence of the Au, C, and O elements, indicating that the surface of the electrode is well covered with gold. The presence of the C element is also related to the GO, rGO and the GS substrate and the element O can be attributed to the slight amount of GOs that are not reduced. For further confirmation, the distribution of the elements performed by the elemental mapping analysis is shown in Figure S2B-D.

As already mentioned, the GO casted onto the electrode surface can be reduced along with the gold reduction by applying successive CVs. This claim can be proved by investigation the FT-IR spectrum of GS/GO presented in the Figure S3. Investigating the FT-IR spectrum of GS/GO (Figure S3a) and comparing it with the GS/GO-Au electrode spectrum (Figure S3c) indicates that the characteristic peaks of GO at 3369, 1726, 1622, 1415, 1215, and 1045 cm^{-1} corresponding to oxygenated functional groups such as OH, C=O, C=C (aromatics), C-O carboxy, C-O (epoxy), and C-O (alkoxy), respectively are almost completely eliminated or their intensity significantly are decreased after deposition of gold. There are two main reasons simultaneously cause obtaining rGO from GO: 1) applying very negative potentials can reduce GO [36, 38]. 2) The presence of gold on the electrode surface serves as a catalyst for the reduction of GO. The FT-IR spectra shows some oxygen-related functional groups such as OH group are still observed even by applying the cycles in the absence of gold under similar conditions (Fig. S3b), however, in the presence of gold, the related absorption bands are reduced or omitted.

This argument is consistent with the previous studies which used metallic nanoparticles such as gold as a catalyst to obtain rGO from GO [39, 40].

The morphology and distribution of elements on the surface significantly depend on the processing conditions [41]. It is possible to simultaneously deposit gold and rGO onto the electrode surface. In that way, GO powder is also added to electrolyte (in the presence of gold) and is dispersed with ultrasonic and finally CV is applied for electrodeposition. In this case, rGO and gold are deposited as layers on the surface and a portion of the gold is buried under rGO (Figure 3A) such that a part of the effective surface area for bonding the bioreceptor is lost. However, if the GO is first drop casted on the surface and then the gold is reduced onto it (as in this study), the presence of the oxygenated functional groups of GO will create sites to form gold structures whereby the gold structures will be exposed. Also, as shown in Figure 3B, gold is not well formed in the absence of GO. In addition, as previously reported, the presence of cysteine is one of the most influential factors on the gold nanostructure [35, 42]. However, when the electrodeposition was carried out in electrolytes containing aqua regia or aqua regia plus H_2SO_4 (in the absence of ammonia), even with cysteine, the desired dendritic structure was not obtained (Figures 3C and D). This can be justified by knowing the fact that cysteine is unstable in the presence of oxidizing agents [43] and also indicates that selecting the appropriate electrolyte is important for achieving an optimal structure. Accordingly, here ammonia was used to balance the solution in terms of pH and to reduce the oxidizing properties of the electrolyte. Probably, cysteine is more stable in the presence of ammonia.

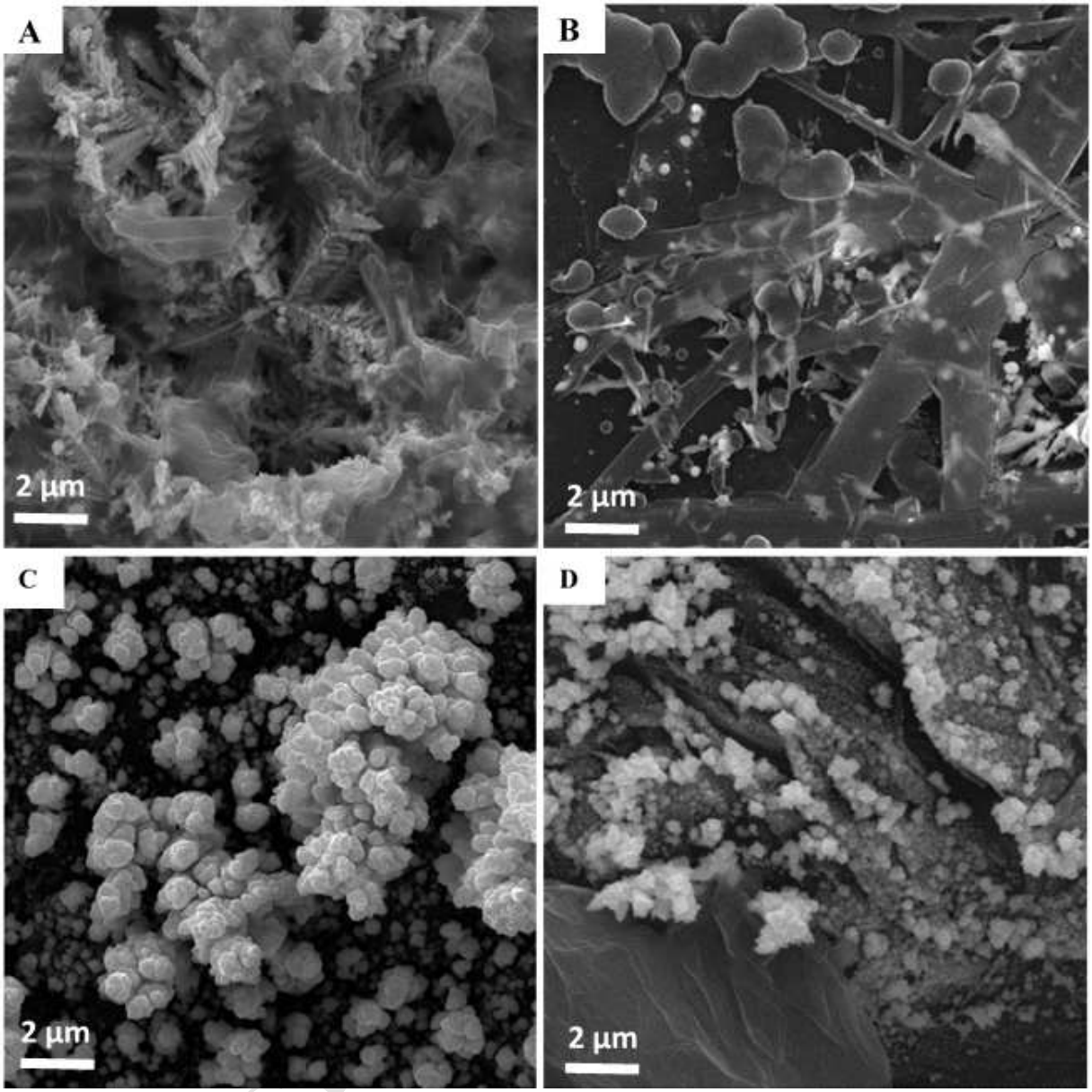

Figure 3. SEM images of different deposition conditions; (A) simultaneously deposition of rGO and Au, (B) electrodeposition of Au on GS in the absence of GO, (C) and (D) electrodeposition in aqua regia and aqua regia containing H_2SO_4, respectively, in the presence of cysteine and absence of NH_3

3.2. Electrochemical behavior of nanocomposite and nanobiosensor

The stability test of the synthesized nanocomposites in the probe solution was performed by applying 10 successive cycles from -0.2 to 0.6 V at the scan rate of 0.05 V s^{-1}. As shown in Figure S4, after consecutive cycles the electrode response remains constant and is very stable. In order to study the properties of different electrodes in each stage of modifications and also to confirm the capturing of HbA1c, CV and EIS tests were performed in the probe solution. The CV curves are shown in Figure 4A. Also, the important parameters of the CVs are extracted and given in Table 1.

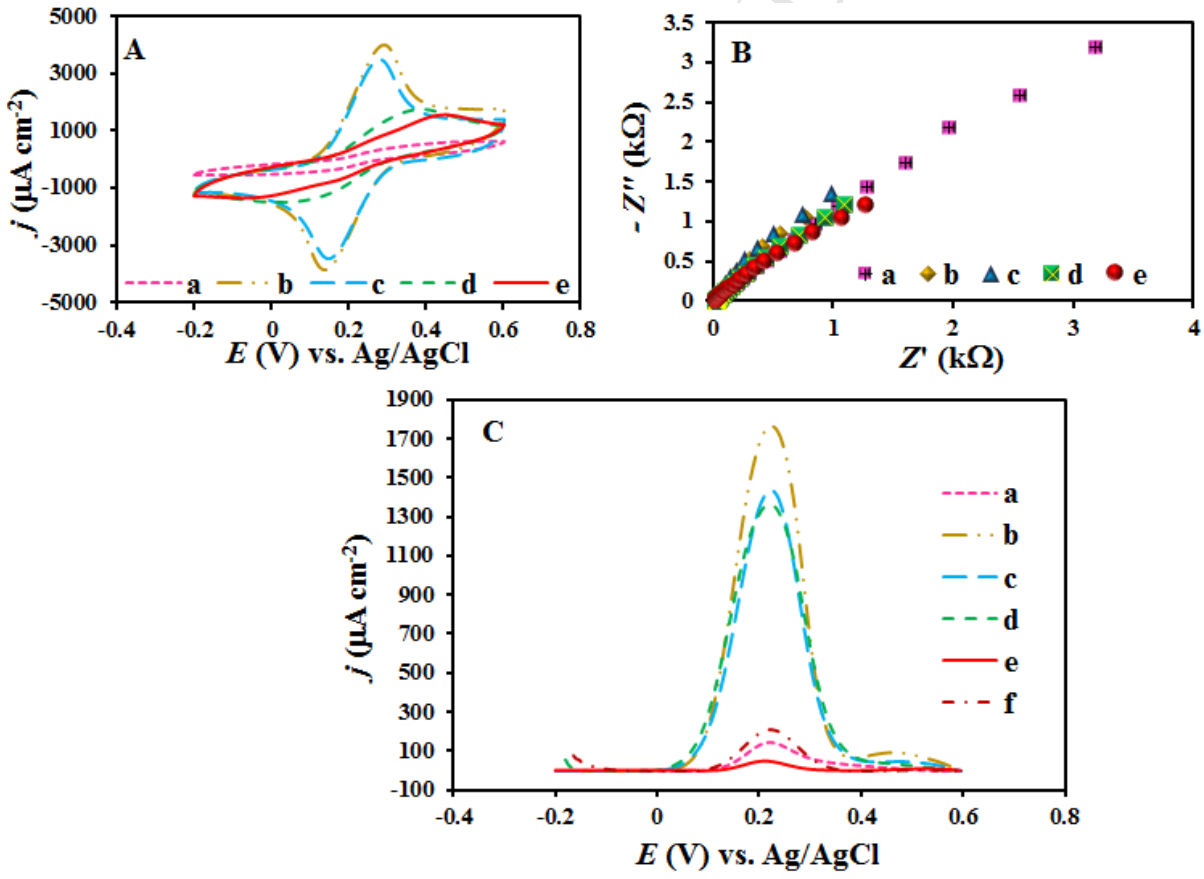

Figure 4. (A) CV curves (B) Nyquist and (C) DPV plots for investigation of different electrodes in each stage of modifications; a) bare GS, b) GS/rGO-Au, c) GS/rGO-Au-aptamer, d) GS/rGO-

Au-aptamer-MU, e) and f) GS/rGO-Au-aptamer-MU-HbA1c (two different concentrations of HbA1c, 13.83 and 1 µmol L^{-1}, respectively) in 0.01 mol L^{-1} PBS solution containing 5 mmol L^{-1} $Fe(CN)_6^{3-}$/ $Fe(CN)_6^{4-}$

Table 1. The important parameters extracted from the CV curves

Electrode	j_{pc} (µA cm^{-2})	j_{pa} (µA cm^{-2})	j_{pc}/j_{pa}	ΔE (V)
Bare GS	-403.52	420.00	-0.96076	0.225
GS/rGO-Au	-3379.32	3310.00	-1.02094	0.146
GS/rGO-Au-aptamer	-2941.08	3037.32	-0.96831	0.125
GS/rGO-Au-aptamer-MU	-921.96	1153.32	-0.7994	0.268
GS/rGO-Au-aptamer-MU-HbA1c	-491.24	754.52	-0.65106	0.415

According to the results, the anodic (i_{pa}) and cathode peak (i_{pc}) currents of the modified electrode with rGO-Au nanocomposite are increased eight times compared with the unmodified electrode and the peak current ratio (i_{pc} / i_{pa}) is equal to unity. This is due to the high surface area and high conductivity of the nanocomposite which facilitates the electron transfer which in turn can improve biosensing properties. The peak potential separation (ΔE_p) also is decreased from 0.225 to 0.146 V indicating an improvement in electron transfer kinetics. However, with the immobilization of aptamer on the electrode surface and treatment with MU as well as the capturing HbA1c, the peak current decreases step by step. Moreover, the anodic and cathodic E_p are clearly shifted toward more positive and negative potentials, respectively, which indicates that the electron transfer kinetics slows down by loading the MU and HbA1c molecules on the electrode surface. This can be explained by the fact that the presence of non-electroactive

molecules on the surface of the electrode (aptamer, MU, HbA1c) blocks the electrode surface and by creating a steric hindrance, a lower surface area of the electrodes is exposed to the redox probe for electron exchange. Lowering the current by binding the DNA aptamer can also be due to the electrostatic repulsion between the negative charge of aptamer sugar-phosphate backbone and the probe molecules ($Fe(CN_6)^{3-/4-}$) [44].

For further studying the interfacial properties of different stages in the construction of nanobiosensor, Nyquist plots of the electrodes were obtained around the peak potential of the nanocomposite-modified electrode (0.269V) (Figure 4B) and the data were fitted with appropriate equivalent circuits. The Nyquist plots for bare GS, GS/rGO-Au and GS/rGO-Au-aptamer were fitted with Randles equivalent circuit (R(QR)). The data is summarized in Table 2 where R_s is the solution resistance, *CPE* or *Q* is a non-ideal capacitance and is a criterion of roughness and heterogeneity of the surface, and R_{ct} is the charge-transfer resistance on the electrode surface. The R_{ct} is improved 7.2 times upon modification of the electrodes with the rGO-Au nanocomposite (it reaches to about 4 kΩ from about 31 kΩ). However, the stabilization of the aptamer increases R_{ct} due to its non-conductivity and the electrostatic repulsion with negative probe molecules. By further treatment of the electrode surface by MU and then capturing HbA1c, the equivalent circuit becomes more complicated (R(Q(RO))) because each of these non-conductive molecules create a capacitor with dielectric properties near the electrode surface. In this system, the cavities and pores between non-conductive molecules can create a pathway for diffusion of the electroactive probe from the bulk of solution to the conductive surface of the electrode which results in the creation of a new interface (electrical double layer) between the

coating and the underlay layer (very conducting nanocomposite). This electrical double layer is formed due to the difference in the concentration of positive and negative ions on both sides of the coating and its dielectric properties. The element *O* in the equivalent circuit of the last two electrodes is related to the constrained diffusion of electroactive molecules from the thin layer. This element is used where the kinetic of the reaction is controlled by slow diffusion of electroactive species. Admittance (*Yo*, Ω^{-1} $s^{1/2}$) and time constant (*B*, $s^{1/2}$) are two characteristic parameters of the *O* element. At high frequency, the behavior of the element *O* is similar to the Warburg impedance. At those frequencies, the frequency of the AC voltage applied is much smaller than the time needed for a molecule to diffuse across the thin layer. In this case, the thickness of the film or coating appears to be large for the diffusing species. This corresponds to the apparent shape of the plot which starts with a straight line. At low frequencies, diffusing species have enough time to pass through the limiting layers and create a resistance [45, 46].

Table 2. Summary of extracted data from Nyquist plots for different electrodes

Electrode	*CPE.Y0* (S-sec^n)	R_{ct} (kΩ)	R_s (Ω)	*CPE.N*	*O-Yo*	*O-B*	Equivalent circuit
Bare GS	0.0002739	31.440	31.32	0.578	-	-	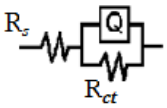
GS/rGO-Au	0.0009542	4.357	28.94	0.785	-	-	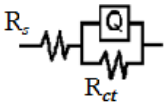
GS/rGO-Au-aptamer	0.0007356	4.726	26.75	0.800	-	-	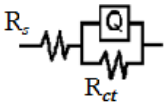
GS/rGO-Au-aptamer-MU	0.0006090	6.507	30.70	0.631	0.00017	1.119	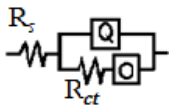
GS/rGO-Au-aptamer-MU-HbA1c	0.0006638	8.950	29.68	0.591	0.01425	0.042	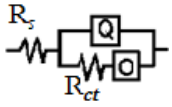

DPV technique was used to investigate and optimize the effect of important parameters. The decrease in the oxidation current of the probe after the affinity capturing of HbA1c with the aptamer immobilized on the electrode surface (i.e, the difference in current density of the biosensor in the absence and presence of the HbA1c molecule (Δj)) was considered as a signal for biosensing. To ensure the sensitivity of the biosensor to changes in HbA1c concentration and to follow the trends of signal variation for a different stage of the modification, DPV curves were recorded for mentioned electrodes and also in the presence of two concentrations of HbA1c (Figure 4C). Decreasing in the signal after each stage of surface modification is in agreement with the results of CV curves and also shows that the biosensor is sensitive to the changes in HbA1c concentration.

In addition, the electron transfer mechanism of the probe at the electrode surface was investigated in the presence and absence of target molecules (HbA1c) by CV test at eight different scan rates from 0.001 to 0.3 V s^{-1} and at the potential range of -0.4 to 0.8 V. The CVs illustrated in Fig. S5A and B represent two oxidation peaks at about 0.3 and 0.7 V that the latter peak shows more incremental changes than the first peak with increasing the scan rate which is probably due to the weak adsorption of the redox probe on the surface of the electrode. Since the adsorption peak current is directly related to the scan rate and the diffusion current is proportional to the square root of the scan rate, this occurrence is justifiable [47]. The exact determination of the height of the second peak current is not possible due to overlapping with the first peak especially when the HbA1c molecule is captured on the surface and also at low scan rates. However, among the plots of Δj versus square root of scan rate and also scan rate for the first pairs of peaks (about 0.3 V), a linear relationship is observed for only the Δj of anodic peak versus square root of scan rate which indicates that the electron transfer mechanism is diffusion-controlled (Figure S5C and D).

It is worth mentioning that in all cases the DPV and CV tests were conducted in PBS solution too and no peak was observed. The curves are not shown, however, a little background current related to non-faradic current was subtracted from the main peak current arising from probe charge transfer. Actually, the electrochemical signal arises from the planar diffusion and electron transfer of electroactive molecules of the probe onto uncoated points of the electrode surface.

3.3. Investigating and optimizing the effects of important parameters

In order to attain the best efficiency of the biosensor for measuring HbA1c, the effect of different parameters such as aptamer concentration, binding time between the aptamer and HbA1c molecule, temperature, and pH was investigated and optimized at a specific concentration of HbA1c (1 μmol L^{-1}). To evaluate repeatability, all tests were repeated three times and the error bars are shown on the corresponding diagrams. Since the concentration of aptamer is one of the important factors for obtaining a well ordered monolayer, the performance of the electrode was tested with various concentrations of aptamer (10^{-10} to 10^{-6} mol L^{-1}). Figure 5A shows the maximum Δj is achieved in 10^{-9} mol L^{-1} concentration of aptamer. At lower concentrations (e.g. 10^{-10} mol L^{-1}) the amount of signal is even lower. This may be due to the inadequate biological elements on the surface to capture more of the HbA1c molecules. Also, at higher concentrations (above 10^{-9} mol L^{-1}) of the aptamer, the signal is first reduced and then levels off. This may be due to interactions between the strands or folding them. Therefore, the active binding sites are not available for capturing HbA1c and they are adsorbed on the surface by nonspecific interactions which are easily removed from the surface by washing. Consequently, the 10^{-9} mol L^{-1} concentration of aptamer was selected for the rest of the tests.

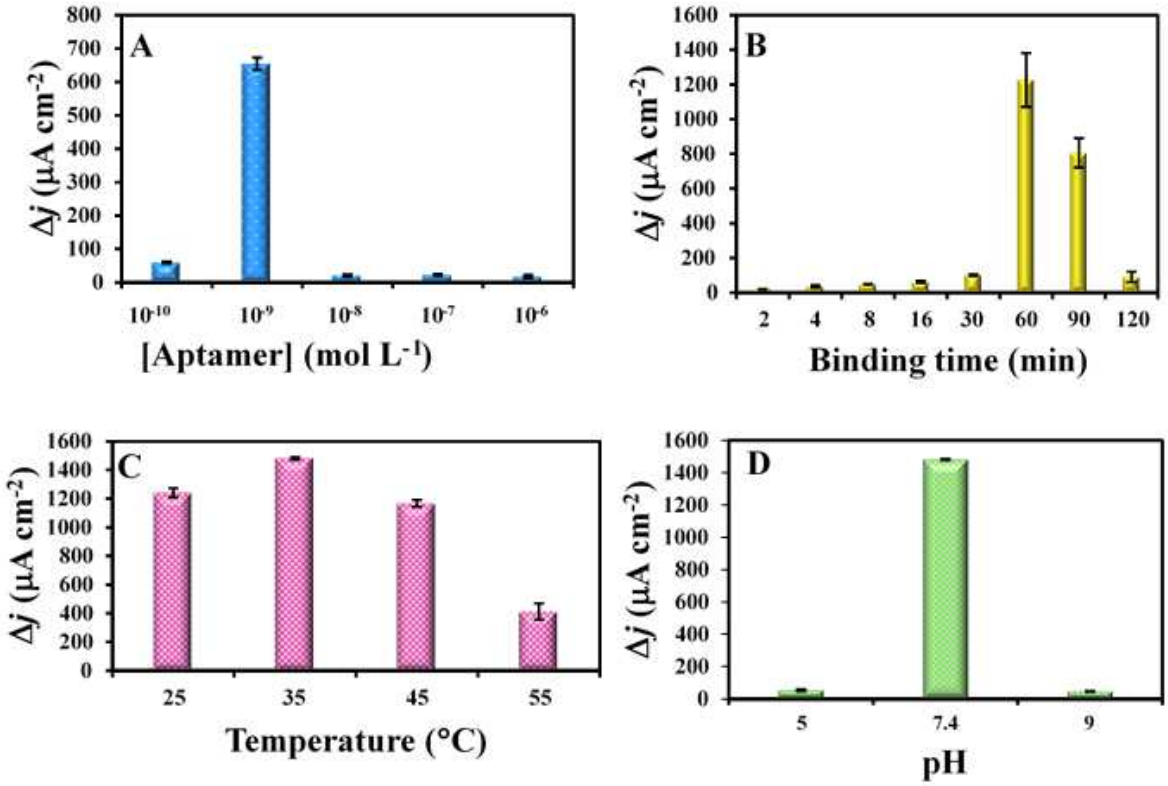

Figure 5. Survey and optimization of significant empirical parameters; (A) concentration of aptamer, (B) binding time of aptamer-HbA1c, (C) temperature of electrochemical cell and (D) pH of sensing solution

The influence of incubation time of the HbA1c and the aptamer to achieve the most effective interaction was investigated in several periods of times from 2 to 120 min (Figure 5B). It is observed that the Δ*j* signal increases with increasing the incubation time up to 60 min and after that decreases which is probably due to the instability of the HbA1c molecule in the ambient temperature at higher incubation times. Therefore, all subsequent experiments were performed in the 60 min of incubation time.

The effect of the electrochemical cell temperature containing $Fe(CN)_6^{3-/4-}$ probe solution on the biosensor response was investigated at several temperature points from 25

to 55 °C. As shown in Figure 5C, the signal increases from 25 to 35 °C and then decreases. This decrease may be due to instability and degradation of the protein molecule and even nucleotide at higher temperatures [48, 49]. Although, the best response of the biosensor was achieved at 35 ° C, other experiments were carried out at ambient temperature to avoid complications for use of the biosensor. Finally, the pH dependence of biosensor performance was revealed by the investigation of the effect of pH at acidic, neutral and basic media (pH=5, 7.4 and 9 respectively). The result depicted in Figure 5D shows that the highest (best response) signal is obtained at neutral pH. Denaturation of nucleic acids and proteins may occur at both acidic and basic pHs. Changing the pH from neutral to acidic or basic can change the surface charge of biomolecules and their intra-molecular bonds can lead to the changing quaternary structure or tertiary structure of biomolecules thus making deformation of active sites and the ineffectiveness of the interactions. Therefore, the normal physiological pH 7.4 was considered as an appropriate value for all of the experiments.

3.4. Dynamic detection range, detection limit, reproducibility and shelf life of the nanobiosensor

For analytical applications and reliability of the responses, there should be a distinct relationship between the observed signal and the target concentration. For investigating this purpose, a series of HbA1c solutions with a specific concentration were used as calibration standards and the biosensor response was recorded under the optimal conditions (Figure 6A). For each HbA1c concentration, the tests were repeated three times. As Figure 6B shows, the plot of Δj against log [HbA1c] has a linear relationship in

a wide range of 1 nmol L^{-1} to 13.83 μmol L^{-1} with extraordinary sensitivity (269.2 μA cm^{-2}) that is still rare in previous literature (Table 4). Since we used calibrator solutions of HbA1c with the highest concentration of 13.83 μmol L^{-1} as standard, the linear range (LR) was limited to this value. The LR may become further wider if the tests can be repeated with higher concentrations of the standards solution in the future. The detection limit was considered as the lowest analyte concentration that can be distinguished from the assay background and experimentally was obtained to be 1 nmol L^{-1}. The reproducibility of the biosensor was evaluated by identical DPV measurements for five same electrodes. The calculated RSD was about 7%, demonstrating a desirable reproducibility for the nanobiosensor and indicating the potential of the electrode for reproducing. The assessment of the biosensor stability for long term storage was followed by testing 6 identical electrodes for five weeks. The electrodes were stored at 4 °C and each week one of them was tested. The biosensor showed satisfactory stability after two weeks of storage and then, its stability was initiated to decline (Figure 6C).

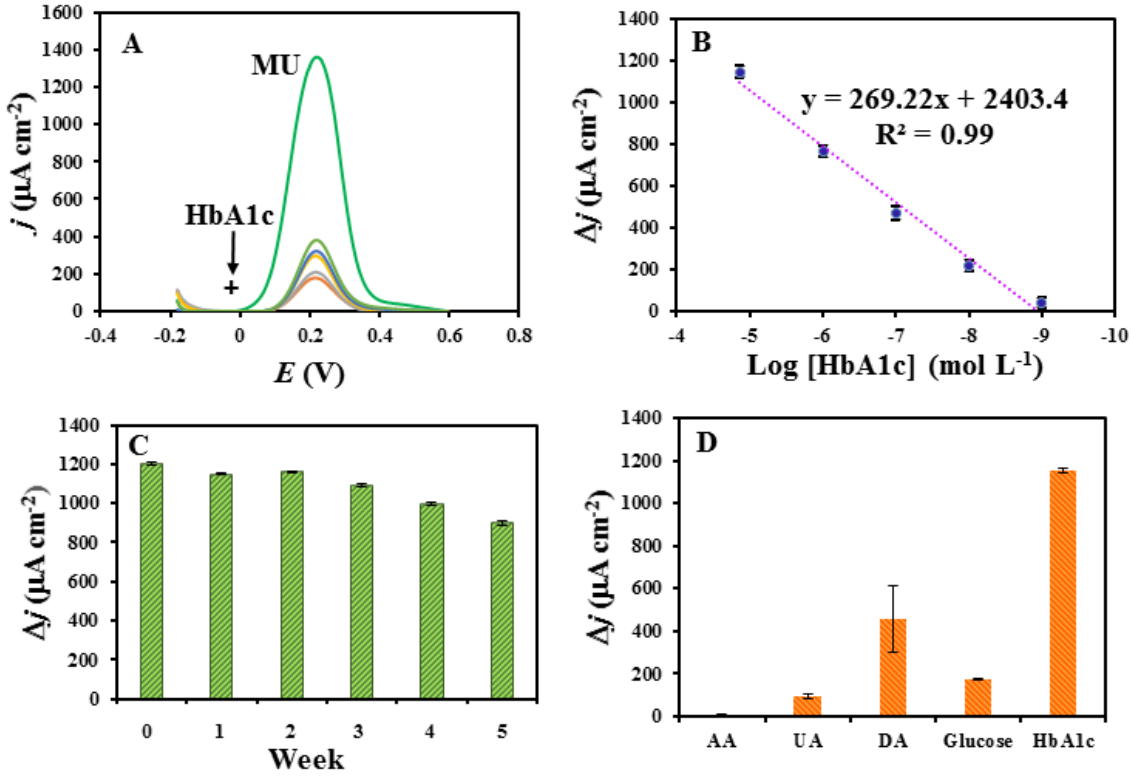

Figure 6. (A) DPV plots of nanobiosensor (GS/rGO-Au-aptamer-MU) at different concentrations of HbA1c, (B) calibration curve for different concentrations of HbA1c, (C) stability assessment of the nanobiosensor for five weeks and (D) selectivity studies of nanobiosensor.

3.5. Selectivity and analytical application of biosensor in real blood sample

In order to assess the biosensor selectivity, its response was investigated against other biomaterials that may be commonly existing in the human blood and are usually investigated by other researchers [18] such as ascorbic acid (AA), uric acid (UA), dopamine (DA) and glucose at the concentration of 100 μM which is equal to or even greater than that in a real blood sample and the results were compared with the nanobiosensor response respect to HbA1c (Figure 6D) [50]. The results showed that in the presence of lower concentration of HbA1c, the obtained signal is even several times higher than those for other materials with higher concentrations. Therefore, it can be concluded that the presence of these materials in the blood sample does not have a significant effect on the performance of the biosensor for measuring the HbA1c. This very high selectivity is due to the use of highly selective aptamer in the biosensor construction.

The efficiency of biosensors in the real samples is a criterion for evaluating their performance. For this purpose, three blood samples remained from routine clinical tests were taken from the Pasteur Institute of Iran. The whole blood specimen was treated with lysis buffer to hemolysis and was diluted with a 0.01 mol L^{-1} PBS solution (pH 7.4), and then a small volume of the treated specimen was tested. The measurements were performed by the nanobiosensor and compared with the laboratory method for the determination of HbA1c. The laboratory report is commonly based on the percentage of HbA1c that measures the amount of HbA1c relative to total Hb. Because the total hemoglobin content of the different individuals varies, total Hb values were also

measured with an autoanalyzer and the amount of HbA1c present in the sample was obtained according to the relationship between HbA1c results from the NGSP network (%HbA1c) and the IFCC network (mmol mol^{-1}) (NGSP = [0.09148 × IFCC] + 2.152) [51]. The results are presented in Table 3. As can be seen, there is a good agreement between the nanobiosensor responses and the standard method which indicates the potential of the biosensor to be used as a part of the HbA1c measurement chip. It is comparable with the previously constructed sensors (Table 4).

Table 3. Application of the constructed biosensor in real blood samples and comparison with a laboratory standard method

Standard method; [HbA1c] (mmol L^{-1})	**Biosensor response; [HbA1c] (mmol L^{-1})**	**Recovery%**	**RSD% (n=3)**
0.051	0.054	105.9	6.09
0.050	0.047	94.0	2.14
0.042	0.046	109.5	7.54

Table 4. Comparison of the response characteristics of the proposed nano-genosensor with some of the previous constructed sensors and biosensors for the HbA_{1C} detection

Electrode and material	Detection method	Bioreceptor	Signaling element	Dynamic range	Limit of detection	Sensitivity	Reference
SPCE/ pTBA@MWCNT[1]	Electrochemical-DPV	aptamer	TBO	0.006 to 0.74 µmol L^{-1}	3.7 nM	1.35, 13.18 µA $µM^{-1}$	[18]
microfluidic chip-magnetic beads	Chemiluminescence	aptamer–antibody	acridinium ester- H_2O_2-NaOH	0.65 to 1.86 g dL^{-1}	0.65 g/dL	50387 a.u./(g dL^{-1})	[33]
SPCE/ AuNPs-pTTBA- APBA[2]	Amperometry	-	H_2O_2	0.1 to 1.5%	0.052 %	2.11 µA/ (mmol mol^{-1})	[52]
Gold electrode/ SAM of T3BA[3]	Electrochemical Impedance Spectroscopy (EIS)	-	-	10 to 100 ng $µL^{-1}$	1 ng/µL	-	[53]
MEMS electrodes/ nanogold capped with mixed SAMs	Potentiometric	antibody	-	50–170.5 ng mL^{-1}	-	58.79, 94.73 µV/(ng mL^{-1})	[54]
GS/rGO-Au nanostructure	Electrochemical-DPV	aptamer	$[Fe(CN)_6]^{3-/4-}$	0.001 to 13.83 µmol L^{-1} (equal to 0.0068 to 94 mg dL^{-1})	1 nmol L^{-1} (equal to 0.0068 mg dL^{-1})	269.2 µA cm^{-2}	This work

[1] Screen printed carbon electrode/ poly(2,2′:5′,5″-terthiophene-3′-*p*-benzoic acid) and a multi-wall carbon nanotube, [2] Screen printed carbon electrode/gold nanoparticles-poly(terthiophene benzoic acid)- aminophenyl boronic acid, [3] Self-assembled monolayer of thiophene-3-boronic acid

4. Conclusion

A disposable electrochemical nanaobiosensor was developed for the determination of HbA1c in blood real samples. The nanobiosensor was fabricated using a paper graphite sheet as an electrode that possesses advantages of convenient to modification, affordability, and availability. A nanocomposite of rGO-gold with hierarchical architecture structure was synthesized by a simple electrochemical protocol to create a substrate for more functionalization to specific capture the target molecule, HbA1c, and also enhance the biosensor performance. This nanostructure gave extraordinary properties to the electrode, providing a repeatable and reproducible measurement with exceptionally high sensitivity in comparison with other biosensors, wide linear range and very low detection limit. However, the blood sample should be diluted because the HbA1c concentration in the blood is greater than the linear range of the biosensor which in turn provides a simpler sample matrix. The nanobiosensor indicated satisfactory stability for a period of time storage. The constructed nanobiosensor has the potential to be used in a point of care chip for screening and monitoring diabetes. Furthermore, other thiolated specific bioreceptors can be tethered on the nanocomposite for the detection of different biomarkers.

Acknowledgment

We gratefully acknowledge the partial support of this work from the Research Council of the Iran University of Science and Technology (160.18130) and Pasteur Institute of Iran.

References

1. Guariguata, L., et al., Diabetes research and clinical practice, 2014. **103**(2): p. 137-149.
2. Boulton, A.J., et al., *Diabetic neuropathies: a statement by the American Diabetes Association.* Diabetes care, 2005. **28**(4): p. 956-962.
3. Forbes, J.M. and M.E. Cooper, *Mechanisms of diabetic complications.* Physiol. Rev., 2013. **93**(1): p. 137-188.
4. Association, A.D., *2. Classification and diagnosis of diabetes.* Diabetes care, 2015. **38**(Supplement 1): p. S8-S16.
5. Syamala Kiran, M., et al., *Selective detection of HbA1c using surface enhanced resonance Raman spectroscopy.* Anal. Chem., 2010. **82**(4): p. 1342-1348.
6. Dong, J., et al., *Simple boric acid-based fluorescent focusing for sensing of glucose and glycoprotein via multipath moving supramolecular boundary electrophoresis chip.* Anal. Chem., 2013. **85**(12): p. 5884-5891.
7. Ang, S.H., et al., *Quantitative, single-step dual measurement of hemoglobin A1c and total hemoglobin in human whole blood using a gold sandwich immunochromatographic assay for personalized medicine.* Biosens Bioelectron., 2016. **78**: p. 187-193.
8. Weykamp, C., *HbA1c: a review of analytical and clinical aspects.* Ann Lab Med, 2013. **33**(6): p. 393-400.
9. Chen, H.-H., et al., *Detection of total and A1c-glycosylated hemoglobin in human whole blood using sandwich immunoassays on polydimethylsiloxane-based antibody microarrays.* Anal. Chem., 2012. **84**(20): p. 8635-8641.
10. Karami, A. and A. Baradaran, *Comparative evaluation of three different methods for HbA1c measurement with High-performance liquid chromatography in diabetic patients.* Adv Biomed Res, 2014. **3**.
11. Dessi, M., et al., *Performances of Capillary Electrophoresis and HPLC Methods in HbA1c Determination: Diagnostic Accuracy in HbS and HbD-Iran Variants' Presence.* J. Clin. Lab. Anal., 2015. **29**(1): p. 57-60.
12. Pundir, C.S. and S. Chawla, *Determination of glycated hemoglobin with special emphasis on biosensing methods.* Anal. Biochem., 2014. **444**: p. 47-56.
13. Yazdanpanah, S., et al., *Glycated hemoglobin-detection methods based on electrochemical biosensors.* TrAC Trends in Anal. Chem., 2015. **72**: p. 53-67.
14. Molazemhosseini, A., et al., *Single-use disposable electrochemical label-free immunosensor for detection of glycated hemoglobin (HbA1c) using differential pulse voltammetry (DPV).* Sensors, 2016. **16**(7): p. 1024.
15. Chopra, A., et al., *Point-of-Care Amperometric Testing of Diabetic Marker (HbA1c) Using Specific Electroactive Antibodies.* Electroanal, 2014. **26**(3): p. 469-472.
16. Stöllner, D., et al., *Membrane-immobilized haptoglobin as affinity matrix for a hemoglobin-A1c immunosensor.* Anal. Chim. Acta, 2002. **470**(2): p. 111-119.
17. Eissa, S. and M. Zourob, *Aptamer-based label-free electrochemical biosensor array for the detection of total and glycated hemoglobin in human whole blood.* Sci Rep., 2017. **7**(1): p. 1016.
18. Moon, J.-M., et al., *A disposable amperometric dual-sensor for the detection of hemoglobin and glycated hemoglobin in a finger prick blood sample.* Biosens Bioelectron., 2017. **91**: p. 128-135.
19. Favero, G., et al., *Electrochemical characterization of graphene and MWCNT screen-printed electrodes modified with AuNPs for laccase biosensor development.* Nanomaterials, 2015. **5**(4): p. 1995-2006.

20. Shahamirifard, S.A., M. Ghaedi, and S. Hajati, *A new silver (I) ions optical sensor based on nanoporous thin films of sol–gel by rose bengal dye.* Sensor Actuat B-Chem, 2018. **259**: p. 20-29.
21. Shahamirifard, S.A. and M. Ghaedi, *Design and construction of a new optical solid-state mercury (II) sensor based on PVC membrane sensitized with colloidal carbon dots.* New J. Chem., 2017. **41**(20): p. 11533-11545.
22. Hong, W., et al., *Preparation of gold nanoparticle/graphene composites with controlled weight contents and their application in biosensors.* J. Phys. Chem. C, 2010. **114** (4): p. 1822-1826.
23. Xu, Y., et al., *Electrodeposition of gold nanoparticles and reduced graphene oxide on an electrode for fast and sensitive determination of methylmercury in fish.* Food Chem., 2017. **237**: p. 423-430.
24. Abraham, S., et al., *Functional graphene–gold nanoparticle hybrid system for enhanced electrochemical biosensing of free cholesterol.* Anal. Methods, 2015. **7**(9): p. 3993-4002.
25. Artiles, M.S., C.S. Rout, and T.S. Fisher, *Graphene-based hybrid materials and devices for biosensing.* Adv. Drug Deliv. Rev., 2011. **63**(14-15): p. 1352-1360.
26. Kuila, T., et al., *Recent advances in graphene-based biosensors.* Biosens Bioelectron., 2011. **26**(12): p. 4637-4648.
27. Diab, N., et al., *A sensitive and selective graphene/cobalt tetrasulfonated phthalocyanine sensor for detection of dopamine.* Sensor Actuat B-Chem, 2019. **285**: p. 17-23.
28. German, N., A. Ramanavicius, and A. Ramanaviciene, *Electrochemical deposition of gold nanoparticles on graphite rod for glucose biosensing.* Sensor Actuat B-Chem, 2014. **203**: p. 25-34.
29. Guo, M.-m., et al., *An ultrasensitive non-enzymatic amperometric glucose sensor based on a Cu-coated nanoporous gold film involving co-mediating.* Sensor Actuat B-Chem, 2014. **203**: p. 388-395.
30. Peng, Y., et al., *Aptamer-gold nanoparticle-based colorimetric assay for the sensitive detection of thrombin.* Sensor Actuat B-Chem, 2013. **177**: p. 818-825.
31. Zhao, Q., et al., *Titania nanotubes decorated with gold nanoparticles for electrochemiluminescent biosensing of glycosylated hemoglobin.* Anal. Chim. Acta, 2016. **936**: p. 83-90.
32. Shahamirifard, S.A., et al., *A simple ultrasensitive electrochemical sensor for simultaneous determination of gallic acid and uric acid in human urine and fruit juices based on zirconia-choline chloride-gold nanoparticles-modified carbon paste electrode.* Biosens Bioelectron., 2018. **114**: p. 30-36.
33. Chang, K.-W., et al., *An integrated microfluidic system for measurement of glycated hemoglobin Levels by using an aptamer–antibody assay on magnetic beads.* Biosens Bioelectron., 2015. **68**: p. 397-403.
34. Hummers Jr, W.S. and R.E. Offeman, *Preparation of graphitic oxide.* J. Am. Chem. Soc., 1958. **80**(6): p. 1339-1339.
35. Lin, T.-H., et al., *Potential-controlled electrodeposition of gold dendrites in the presence of cysteine.* ChemComm, 2011. **47**(7): p. 2044-2046.
36. Ghiabi, C., et al., *In situ, one-step and co-electrodeposition of graphene supported dendritic and spherical nano-palladium-silver bimetallic catalyst on carbon cloth for electrooxidation of methanol in alkaline media.* RENEW ENERG, 2018. **126**: p. 1085-1092.

37. Yang, J., et al., *Electrochemical synthesis of reduced graphene sheet–AuPd alloy nanoparticle composites for enzymatic biosensing.* Biosens Bioelectron., 2011. **29**(1): p. 159-166.
38. Guo, H.-L., et al., *A green approach to the synthesis of graphene nanosheets.* ACS nano, 2009. **3**(9): p. 2653-2659.
39. Zhuo, Q., et al., *Large-scale synthesis of graphene by the reduction of graphene oxide at room temperature using metal nanoparticles as catalyst.* Carbon, 2013. **52**: p. 559-564.
40. Hurtado, R.B., et al., *One-step synthesis of reduced graphene oxide/gold nanoparticles under ambient conditions.* Arab. J. Chem., 2017.
41. Soleymani, L., et al., *Nanostructuring of patterned microelectrodes to enhance the sensitivity of electrochemical nucleic acids detection.* Angew, 2009. **48**(45): p. 8457-8460.
42. Tran, M., et al., *Electrodeposition of Gold Nanostructures Having Controlled Morphology.* J. Nanosci. Nanotechnol., 2018. **18**(5): p. 3492-3498.
43. Hamann, M.J., *Irreversible oxidation of protein cysteine residues.* 2002.
44. Silva, M.M., et al., *Gold electrode modified by self-assembled monolayers of thiols to determine DNA sequences hybridization.* J. Chem. Sci., 2010. **122**(6): p. 911-917.
45. Jacobsen, T. and K. West, *Diffusion impedance in planar, cylindrical and spherical symmetry.* Electrochim. Acta, 1995. **40**(2): p. 255-262.
46. Freger, V., *Diffusion impedance and equivalent circuit of a multilayer film.* Electrochem. commun., 2005. **7**(9): p. 957-961.
47. Bard, A.J. and L.R. Faulkner, *Fundamentals and applications.* Electrochemical Methods, 2001. **2**: p. 482.
48. Deng, H., et al., *Quantum dots-labeled strip biosensor for rapid and sensitive detection of microRNA based on target-recycled nonenzymatic amplification strategy.* Biosens Bioelectron., 2017. **87**: p. 931-940.
49. Salahandish, R., et al., *Nano-biosensor for highly sensitive detection of HER2 positive breast cancer.* Biosens Bioelectron., 2018.
50. Esmaeeli, A., et al., *Copper oxide-polyaniline nanofiber modified fluorine doped tin oxide (FTO) electrode as non-enzymatic glucose sensor.* Sensor Actuat B-Chem, 2018. **266**: p. 294-301.
51. Hoelzel, W., et al., *IFCC reference system for measurement of hemoglobin A1c in human blood and the national standardization schemes in the United States, Japan, and Sweden: a method-comparison study.* Clin Chem., 2004. **50**(1): p. 166-174.
52. Kim, D.-M. and Y.-B. Shim, *Disposable amperometric glycated hemoglobin sensor for the finger prick blood test.* Anal. Chem., 2013. **85**(13): p. 6536-6543.
53. Hsieh, K.-M., et al., *Glycated hemoglobin (HbA1c) affinity biosensors with ring-shaped interdigital electrodes on impedance measurement.* Biosens Bioelectron., 2013. **49**: p. 450-456.
54. Xue, Q., et al., *A micro potentiometric immunosensor for hemoglobin-A1c level detection based on mixed SAMs wrapped nano-spheres array.* Biosens Bioelectron., 2011. **26**(5): p. 2689-2693.

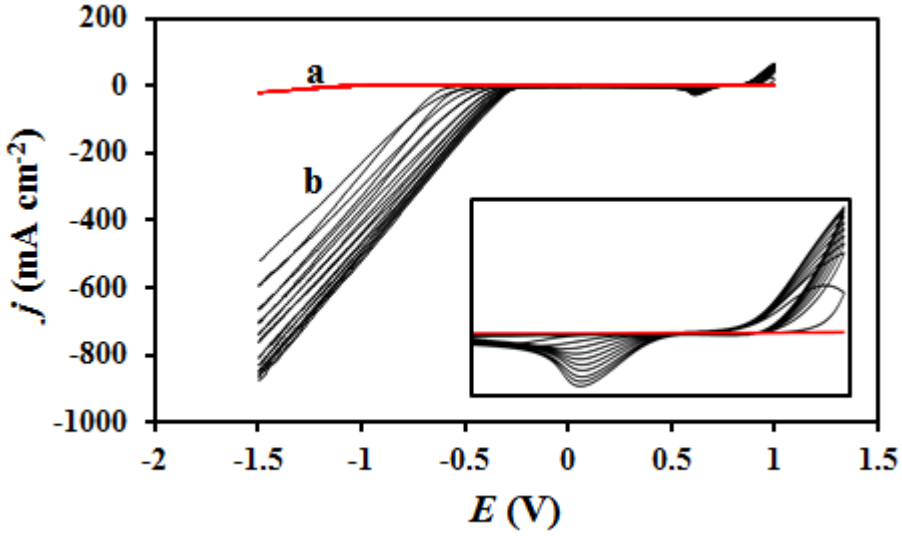

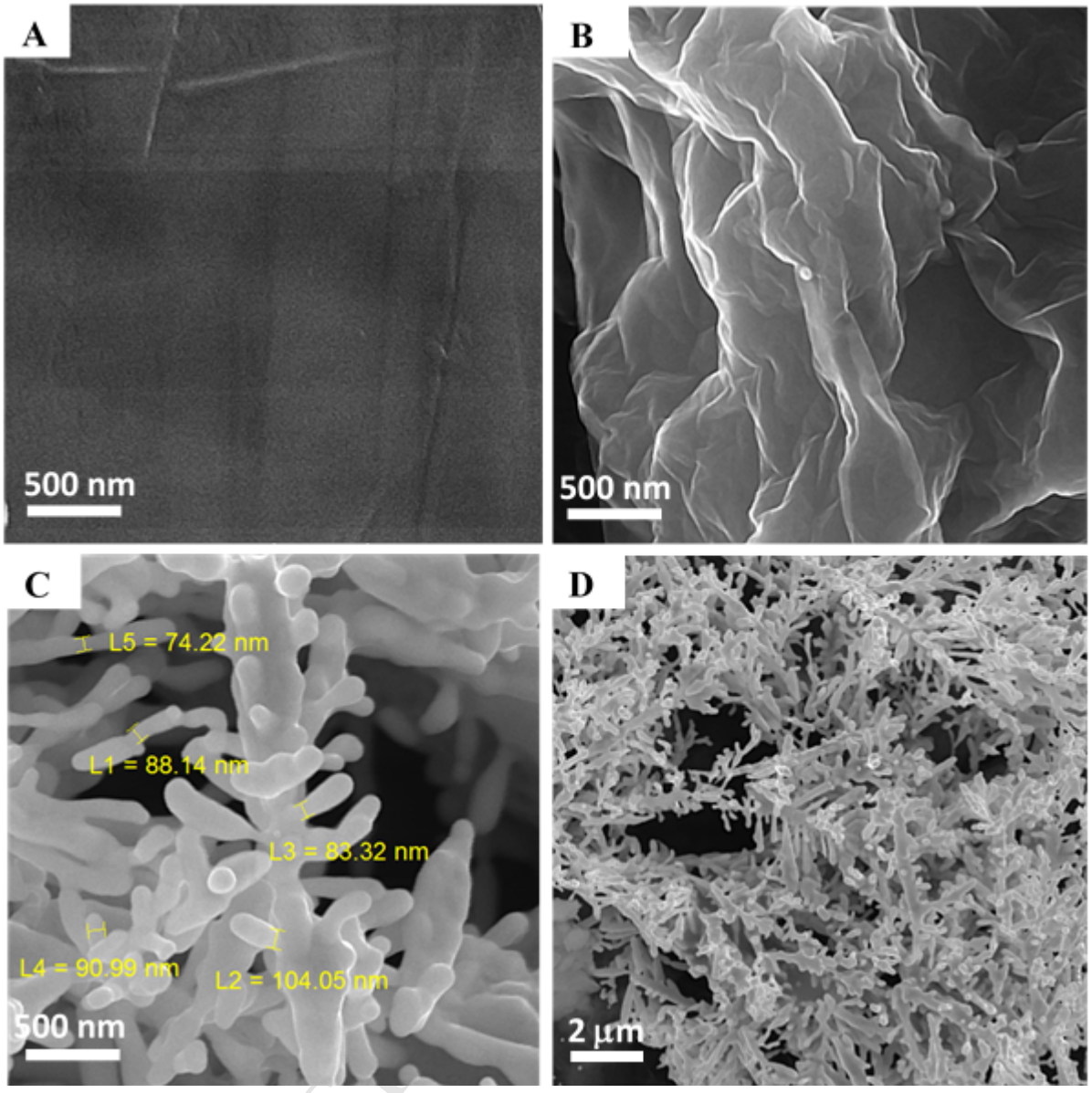
A
500 nm
B
500 nm
C
L5 = 74.22 nm
L1 = 88.14 nm
L3 = 83.32 nm
L4 = 90.99 nm
L2 = 104.05 nm
500 nm
D
2 μm

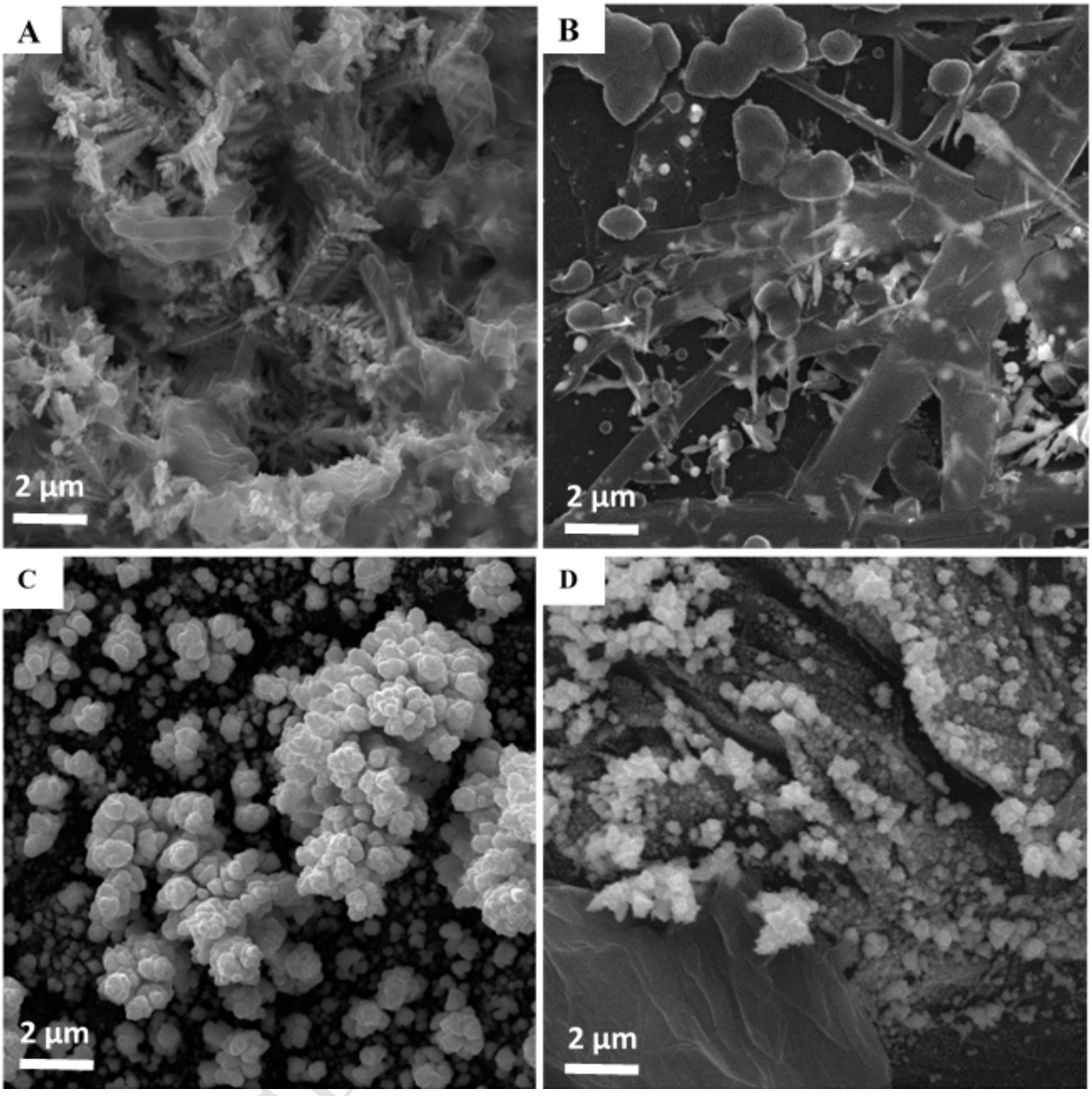

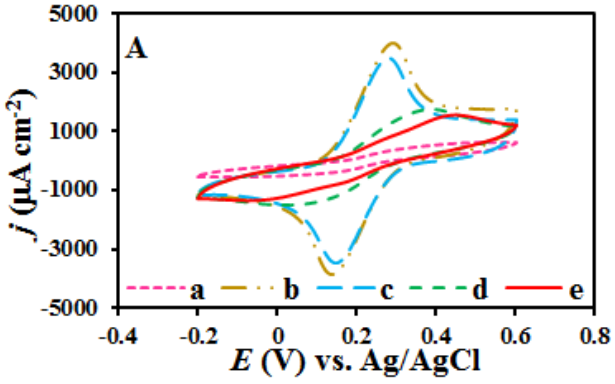

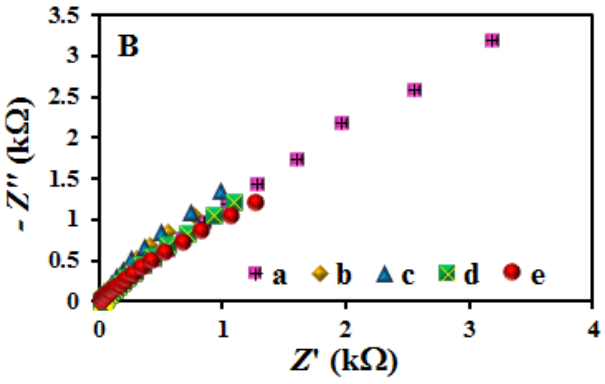

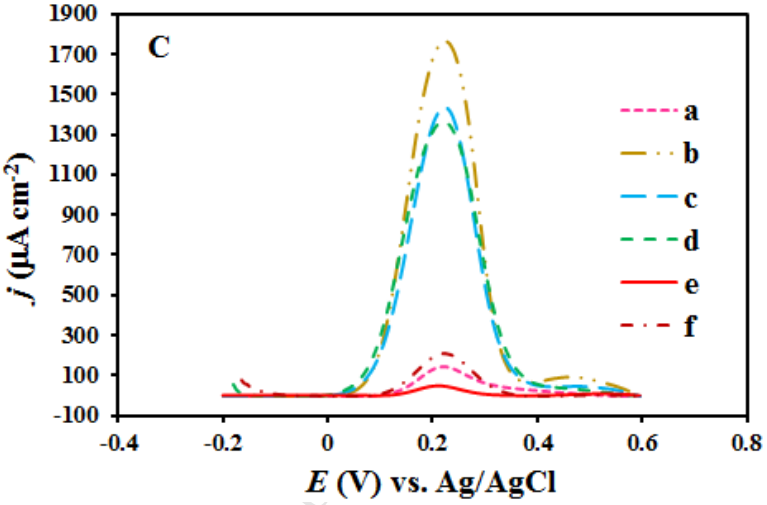

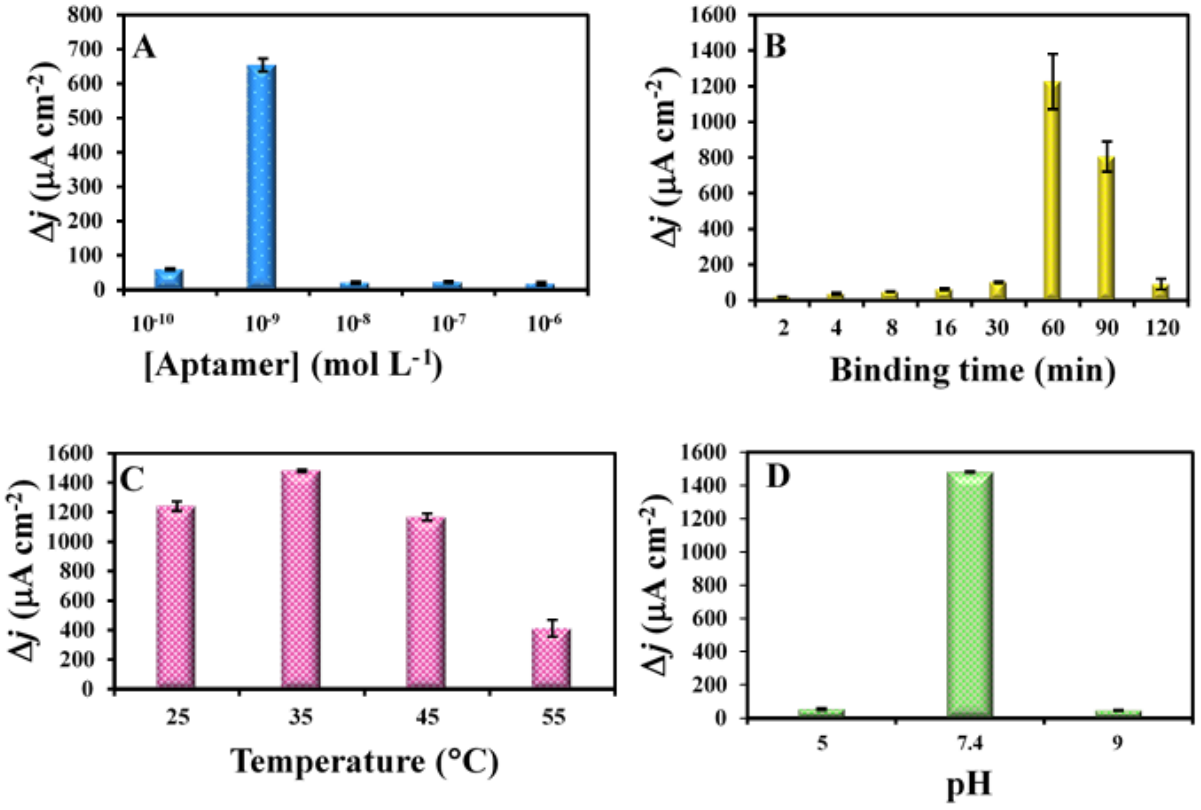

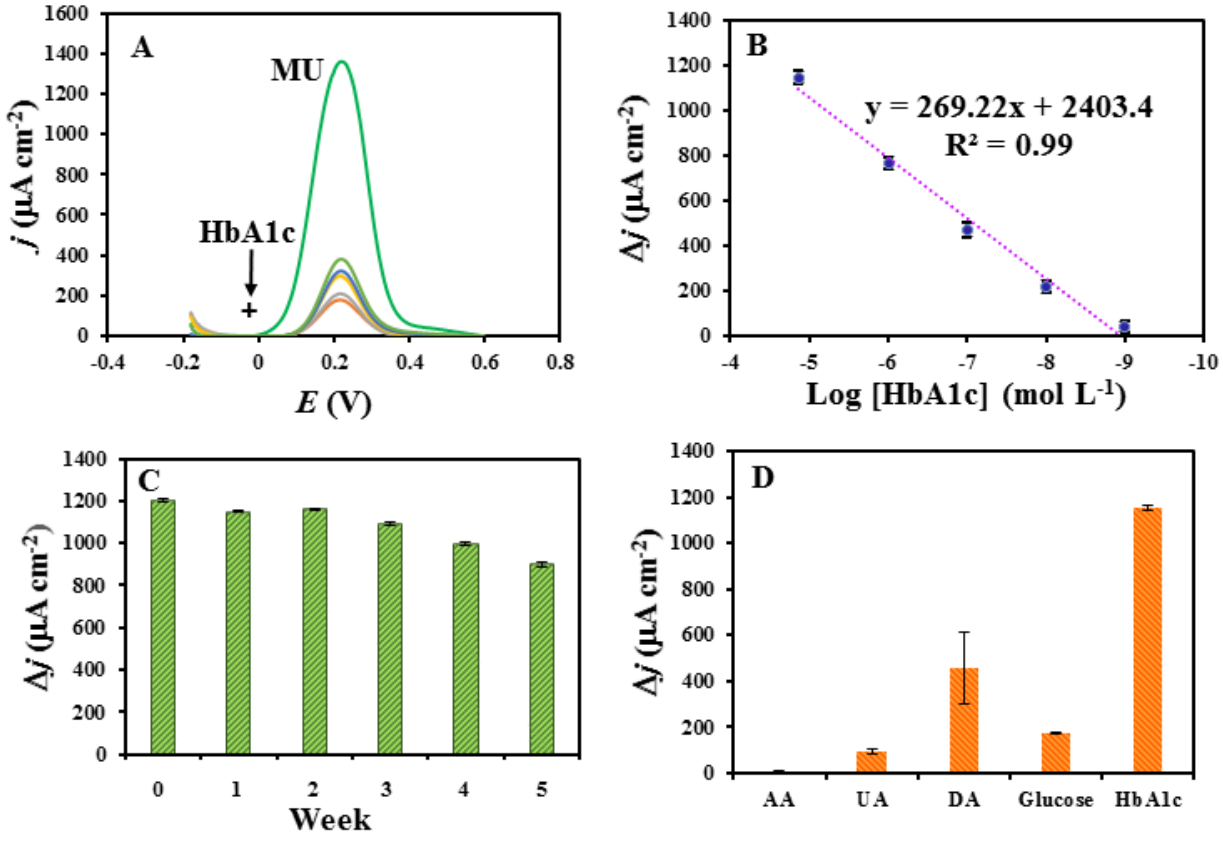

Highlights

- An electrochemical nano-genosensor is proposed to hemoglobin A1c determination.
- Graphite sheet (GS) is used as a cheap electrode and good candidate to commercialize
- A nanostructure of RGO-gold is electrodeposited on the GS by a facile method.
- The biosensor exhibited a very high sensitivity for measuring HbA1c.
- The developed biosensor is successfully used for HbA1c measurement in blood sample.

Declaration of interests

☒ The authors declare that they have no known competing financial interests or personal relationships that could have appeared to influence the work reported in this paper.

☐The authors declare the following financial interests/personal relationships which may be considered as potential competing interests:

Declaration of interests

☒ The authors declare that they have no known competing financial interests or personal relationships that could have appeared to influence the work reported in this paper.

☐The authors declare the following financial interests/personal relationships which may be considered as potential competing interests: